



Numerical investigation of a wind turbine rotor with an aerodynamically redesigned hub-region

Johansen, J.; Aagaard Madsen, H.; Sørensen, Niels N.; Bak, C.

Published in:

European Wind Energy Conference and Exhibition 2006, EWEC 2006

Publication date:

2006

Document Version

Peer reviewed version

[Link back to DTU Orbit](#)

Citation (APA):

Johansen, J., Aagaard Madsen, H., Sørensen, N. N., & Bak, C. (2006). Numerical investigation of a wind turbine rotor with an aerodynamically redesigned hub-region. In *European Wind Energy Conference and Exhibition 2006, EWEC 2006* (Vol. 2, pp. 1694-1702). European Wind Energy Association (EWEA).

General rights

Copyright and moral rights for the publications made accessible in the public portal are retained by the authors and/or other copyright owners and it is a condition of accessing publications that users recognise and abide by the legal requirements associated with these rights.

- Users may download and print one copy of any publication from the public portal for the purpose of private study or research.
- You may not further distribute the material or use it for any profit-making activity or commercial gain
- You may freely distribute the URL identifying the publication in the public portal

If you believe that this document breaches copyright please contact us providing details, and we will remove access to the work immediately and investigate your claim.

Numerical Investigation of a Wind Turbine Rotor with an aerodynamically redesigned hub-region

J. Johansen, H. A. Madsen, N. N. Sørensen and C. Bak
Wind Energy Dept.
Risø National Laboratory
Roskilde, Denmark
jeppe.johansen@risoe.dk

Abstract:

The effect of increasing the blade chord and twist distribution of the blade in the vicinity of the wind turbine nacelle, to obtain an aerodynamically more efficient rotor is investigated using three different aerodynamic methods, i.e. Blade Element Momentum (BEM) method, Actuator Disc (AD) method and a full 3D Navier-Stokes (NS) solver.

On most wind turbines the inner part of the rotor is designed based mainly on structural issues since it is believed that the amount of produced power in the inner part of the rotor is insignificant and does not have an influence on the energy conversion further outboard on the blade. This has led to a design where the root chord has been limited in size due to structural considerations.

Recently, increased power coefficients are reported¹ on a rotor with increased chord and twist at the inner part of the blade in combination with a large diameter spinner, compared to a more conventional design.

The present paper describes a numerical investigation of a new blade design with an aerodynamically redesigned hub-region compared with a traditional rotor design using BEM, AD and 3D NS.

The paper includes comparisons of produced mechanical power and thrust coefficients, radial distribution of local power and thrust coefficients, as well as flow visualisations compared to a traditional rotor design.

Results show that local C_p differs considerably on the inner part of the rotor using the proposed blade design when comparing BEM with more complex methods as AD and 3D NS. Global C_p and C_T increase only slightly indicating complex spanwise dependency not accounted for in BEM methods. This could lead to design changes in future rotor designs.

Keywords: rotor aerodynamics, CFD, power coefficient.

1 Introduction

The background for the present work is a publication from a wind turbine manufacture saying that a new aerodynamically optimal rotor design can achieve a considerably higher yield. In ref. [1] it is stated that for the new 2 MW ENERCON E-70 (71 m rotor diameter) “*the new blades generate a measured and certified increased yield of 12-15 per cent compared to neighbouring E-66/20.70 (70 m rotor diameter)*”. The explanation is according to ref. [1] that “*the new blade root section which closes off directly on the spinner is extremely deep and therefore reaps additional wind from two sides.*” Additional changes to the blade design include more slender blades on the outer part as well as a new optimized blade tip.

It is well known that state-of-the-art aerodynamic models for wind turbine rotor design have their limitations. The flow right behind the rotor is highly three-dimensional and most rotor design methods do not correctly take these effects into account. Especially in the root region where spanwise flow is often present on conventional turbines. Using BEM the local power coefficient, C_p , $\rightarrow 0$ when the local tip speed ratio, $\lambda = r\Omega/W \rightarrow 0$. de Vries² shows that including the effect of wake expansion together with the deficit of the static pressure in the wake, C_p can exceed the Betz limit when $\lambda \rightarrow 0$. This effect is not taken into account in standard BEM methods, which could result in non-optimal blade design of the inner part of the blade.

The purpose of the present work is to investigate whether an increase in chord and twist distribution will result in an increase in global C_p . The paper describes aerodynamic computations using three different aerodynamic methods on a redesigned modern Mega-Watt sized wind turbine, where the new design includes an increase in chord and twist distribution on the inner part of the blade. Additionally, the effect of including an egg-shaped spinner is investigated.

2 Methods

The analysis is based on the results obtained using three different aerodynamic methods, namely a standard Blade Element Momentum (BEM) method, an Actuator Disc (AD) method and a full 3D Navier-Stokes solver, EllipSys3D.

2.1 Blade Element Momentum method

Comparisons are made to computations using the HAWC³ code, where the aerodynamics is modeled on basis of the Blade Element Momentum (BEM) method. See e.g. Glauert⁴ for details on BEM. In standard BEM methods the rotor disc is divided into N annular elements, where the flow in each element is computed independently from its neighboring elements. I.e. spanwise effects are not accounted for. Also a cylindrical wake is assumed.

In the present code Prandtl's tip correction is included for correct treatment of the flow near the tip and Glauert's empirical formula is applied for high axial induction factors.

2.2 Actuator Disc solver

In the second aerodynamic method an Actuator Disc (AD) model is used for computations of the induction. Still the basic code for the computations is the HAWC code but now coupled to an Actuator Disc, where the flow field is computed with a Navier-Stokes Solver. The AD model replaces thus the BEM model in this case.

The AD model coupled to the HAWC code has previously been used to analyze yawed flow aerodynamics⁵ and ⁶, and in this case a 3D AD model was used. However in the present case the simulations have been run using a cylindrical AD flow model but including swirl of the flow. There are thus less assumptions and limitations in the computations of the flow field through the Actuator Disc as is present in the BEM method.

It should be noted that both the BEM method and the AD method needs as input a set of airfoil data and an identical set has been used for the two methods

2.3 Navier-Stokes solver, EllipSys3D

Finally, The NS solver, EllipSys3D is used for the full 3D NS wind turbine rotor computations. The Computational Fluid Dynamics (CFD) code is developed by Michelsen^{7,8} and Sørensen⁹ and is a multiblock finite volume discretization of the incompressible Reynolds Averaged Navier-Stokes equations in general curvilinear coordinates. The code uses a collocated variable arrangement, and Rhie/Chow interpolation is used to avoid odd/even pressure decoupling. As the code solves the incompressible flow equations, no equation of state

exists for the pressure and the SIMPLE algorithm is used to enforce the pressure/velocity coupling. The EllipSys3D code is parallelized with MPI for executions on distributed memory machines, using a non-overlapping domain decomposition technique. Solution of the momentum equations is obtained using a third order quadratic upwind interpolation scheme (QUICK) for the convective terms. All computations are performed assuming steady state conditions with a moving mesh technique based on analytical prescribed rotation¹⁰. The turbulent eddy viscosity is modeled using the $k-\omega$ SST model by Menter¹¹. The inflow velocity is constant, with zero shear and has a low turbulence intensity.

A large effort has been put in generating the computational mesh, where various grid topologies have been tested. The final grid topology on the rotor geometry with spinner is shown in Figure 1. The surface mesh is generated using Gridgen, a commercial mesh generator developed by Pointwise, Inc. and consists of 108 blocks of 32^2 cells for the rotors without spinner and 156 blocks of 32^2 cells for the rotors with spinner. The difference in amount of cells is due to the resolution of the spinner. The grid density on the blades is identical. The volume mesh is generated using Risø's in-house grid generator HypGrid¹² and away from the surface 128 cells are used resulting in $20.4 \cdot 10^6$ cells in total for the largest mesh. The grid density used is based on more than 10 years of experience in rotor computations. No-slip is assumed on the entire geometry. (I.e. also the aft part of the spinner is rotating in contrast to real application.) The outer boundary of the computational domain is placed approximately five rotor diameters away.

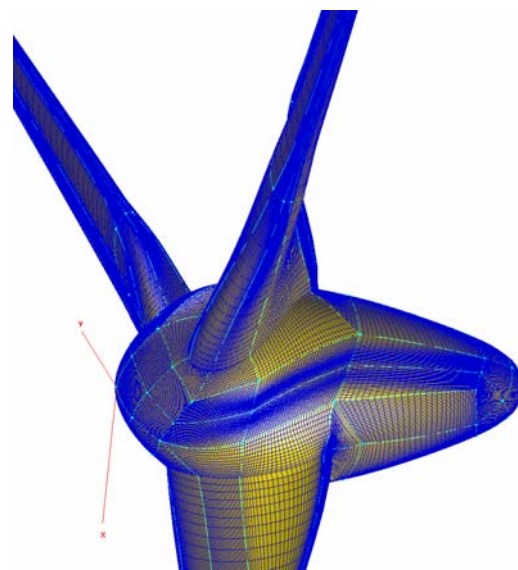


Figure 1: Surface mesh topology on the rotor with spinner.

To investigate the effect of the spinner a special rotor was designed, where the spinner was removed and the new blade design was continued all the way to the rotation centre, but twisted to 90° to reduce the loading, Figure 2.

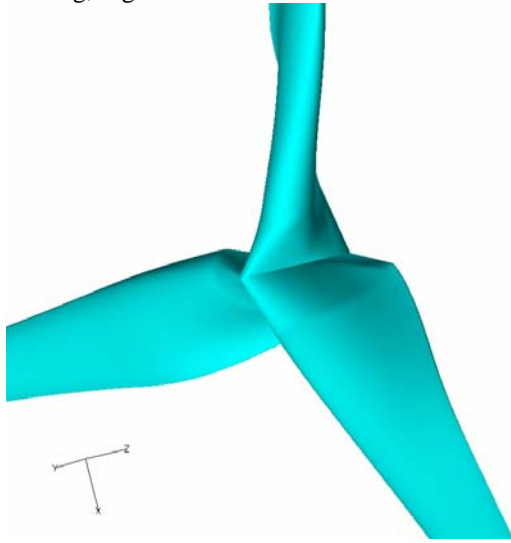


Figure 2: Rotor geometry of new design without spinner.

3. Results

A modern Mega-Watt type wind turbine rotor has been redesigned having an increased chord and twist distribution at the innermost approx. 30 % of the blades. It should be noted that the new design is based on simple Blade Element Momentum considerations and do not take into account the spanwise coupling at the root. Figure 3 and Figure 4 show the change of chord and twist distribution, respectively, on the inner 50 % of the blade. The chord and the twist have been non-dimensionalised as well as the innermost part of the twist has been replaced by a smooth curve for confidentiality reasons.

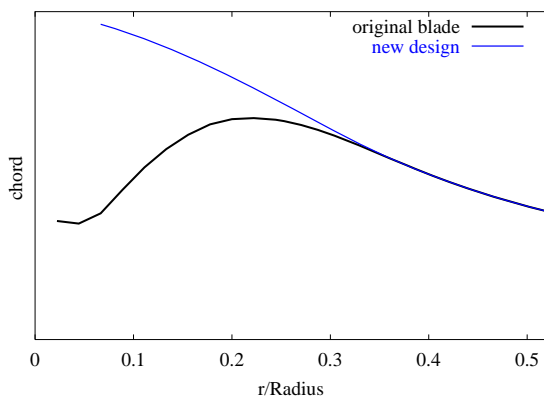


Figure 3: Chord distribution of the innermost 50% of the new blade compared with the original blade.

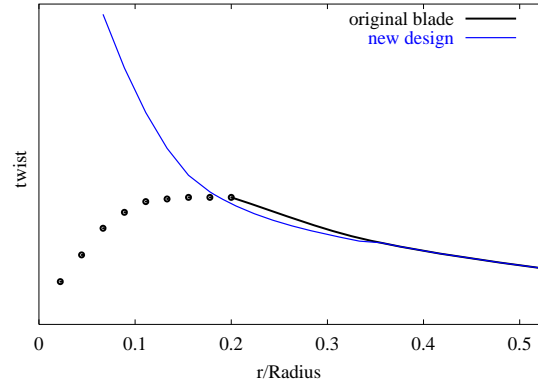


Figure 4: Twist distribution of the innermost 50% of the new blade compared with the original blade.

Additionally, the effect of having an egg-shaped spinner is investigated to see if the speed-up around the spinner influences the performance on the inner part of the rotor. The radius of the spinner is approx. 7 % of the rotor radius.

Three wind speeds have been computed, i.e. $W = 8, 10$ and 12 m/s keeping the pitch setting and rotational speed constant.

Results are presented as global power and thrust coefficients, C_P and C_T , as well as local power and thrust coefficients C_{p_i} and C_{t_i} , respectively, along the blade span. Finally, contour plots and visualizations of limiting streamlines are shown.

The following two tables show global C_P and C_T , respectively, computed using the three different aerodynamic methods.

Table 1: Mechanical power coefficient C_P computed using BEM, Actuator Disc and EllipSys3D. % increase is shown in ().

Wind speed	Original blade	New design w.o. spinner	New design w. spinner
BEM			
8 m/s	0.507	0.512 (+1.0 %)	n.a.
10 m/s	0.472	0.478 (+1.3 %)	n.a.
12 m/s	0.409	0.416 (+1.7 %)	n.a.
Actuator Disc			
8 m/s	0.528	0.530 (+0.4 %)	0.529 (+0.2 %)
10 m/s	0.491	0.496 (+1.0 %)	0.492 (+0.2 %)
12 m/s	0.419	0.425 (+1.4 %)	0.422 (+0.7 %)
EllipSys3D			
8 m/s	0.501	0.506 (+1.0 %)	0.501 (+0.0 %)
10 m/s	0.475	0.480 (+1.0 %)	0.482 (+1.5 %)
12 m/s	0.400	0.414 (+3.5 %)	0.411 (+2.8 %)

Table 2: Thrust coefficient C_T computed using BEM, Actuator Disc and EllipSys3D. % increase is shown in ().

Wind speed	Original blade	New design w.o. spinner	New design w. spinner
BEM			
8 m/s	0.844	0.853 (+1.1 %)	n.a.
10 m/s	0.692	0.702 (+1.4 %)	n.a.
12 m/s	0.574	0.583 (+1.6 %)	n.a.
Actuator Disc			
8 m/s	0.861	0.869 (+0.9 %)	0.866 (+0.6 %)
10 m/s	0.706	0.717 (+1.6 %)	0.712 (+0.8 %)
12 m/s	0.581	0.590 (+1.5 %)	0.586 (+0.9 %)
EllipSys3D			
8 m/s	0.842	0.850 (+1.0 %)	0.850 (+1.0 %)
10 m/s	0.693	0.704 (+1.6 %)	0.711 (+2.6 %)
12 m/s	0.556	0.576 (+3.6 %)	0.576 (+3.6 %)

Because the difference is quite small C_p and C_T are given with three digits even though the uncertainty is not that small.

In general, all three aerodynamic models predict an increase in C_p and C_T for the new design without spinner with 12 m/s giving the largest relative increase. The new design with spinner also show a small increase but not as large as without spinner.

The design with the spinner is not computed using the BEM method since the speed up of the flow is not accounted for in the present implementation of the BEM method.

Local power coefficient C_p

The local power coefficient, C_p , is defined as

$$C_p = \frac{rBF_\theta\Omega\Delta r}{\frac{1}{2}\rho W^3 2\pi r\Delta r},$$

where F_θ is the local tangential force pr. length, B is the number of blades, Ω is the rotational speed and Δr is the width of the local blade section. Plotting C_p as function of rotor radius several observations are made.

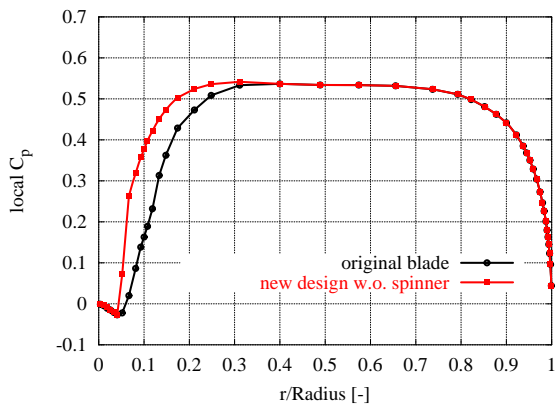


Figure 5: Local C_p distribution, $W= 10$ m/s, BEM.

Figure 5 shows the local C_p computed using the BEM method for the new design compared with the original design. It is seen that the new design results in an increase in local C_p where the chord and twist are increased, as expected. Also, no effect is seen further outboard since the BEM method is radially independent.

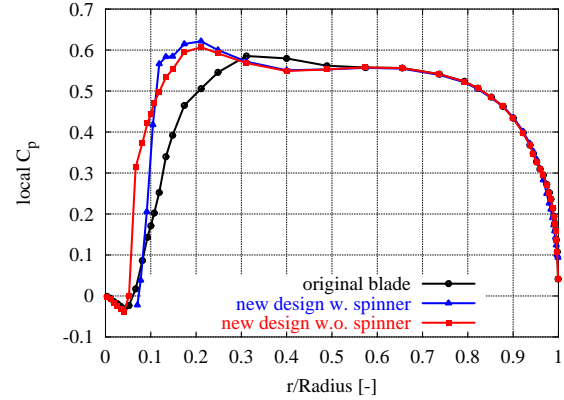


Figure 6: Local C_p distribution, $W= 10$ m/s, Actuator Disc.

Using the AD method larger effects are observed. Figure 6 shows again the local C_p at 10 m/s using the AD method. Here the computation on the new design including the spinner is included. An increase in C_p up to above 0.6 on the innermost 30 % is obtained with the new design. The increased chord results in an increased local solidity, which directly causes an increase in thrust (see below), which again will lead to an increase in local power. At 30-50% rotor radius the local C_p is actually reduced compared to the original blade indicating that the problem is highly three-dimensional in the way that changes on one part of the blade can change the conditions on another part of the blade.

Including the spinner the effect is even larger. (C_p is not computed on the spinner.)

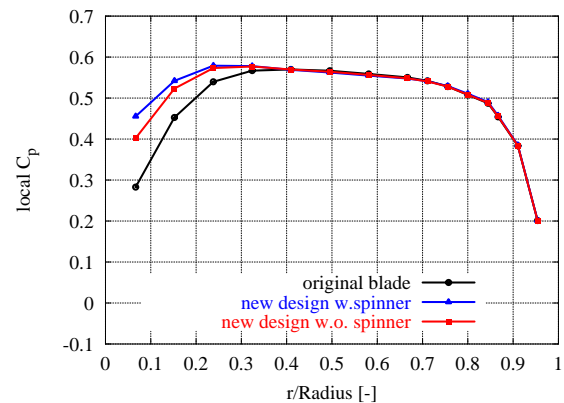


Figure 7: Local C_p distribution, $W= 10$ m/s, EllipSys3D.

Looking at the full 3D NS computations, Figure 7, it is seen that the new design does increase the local C_p on the inner part, but not as much as the AD method. Again, small reduction further outboard is observed underlining the complexity of the three-dimensional flow.

Local thrust coefficient C_t

The following three figures show the local thrust force coefficients, C_t , defined as

$$C_t = \frac{F_t \Delta r}{\frac{1}{2} \rho W^2 2\pi r \Delta r},$$

where F_t is the local thrust force pr. length, as function of rotor radius.

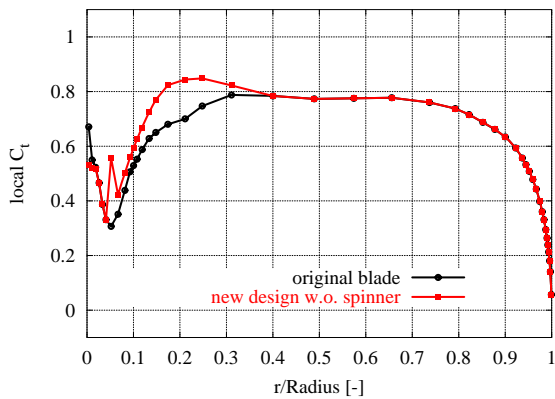


Figure 8: Local C_t distribution, $W= 10$ m/s, BEM.

Figure 8 shows C_t obtained using BEM method. Again the increased thrust is directly a result of the large chord near the root.

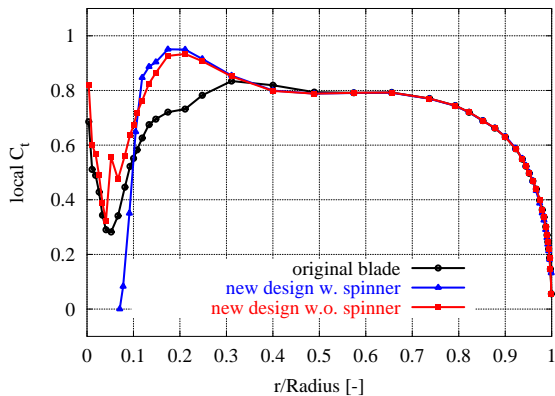


Figure 9: Local C_t distribution, $W= 10$ m/s, Actuator Disc.

Figure 9 shows C_t obtained using the AD method. The local C_t is further increased using the AD method compared to the BEM results.

Finally, the EllipSys3D results are shown in Figure 10. Again one sees an increase in local thrust coefficient with the new design, with a small further increase with spinner.

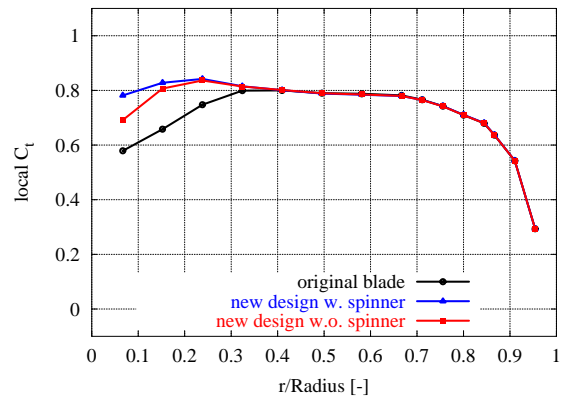


Figure 10: Local C_t distribution, $W= 10$ m/s, EllipSys3D.

Contour plots

To further analyze the flow, contour plots in a vertical plane through the rotor are shown (one blade is pointing upwards and intersects with the vertical plane.) The following three figures show the pressure contours computed using the EllipSys3D code. Wind is blowing from left to right at 8 m/s. The blue color indicates low pressure. All rotors show a low-pressure region downstream along the rotation centre, but the new design with spinner shows the lowest pressure in this region.

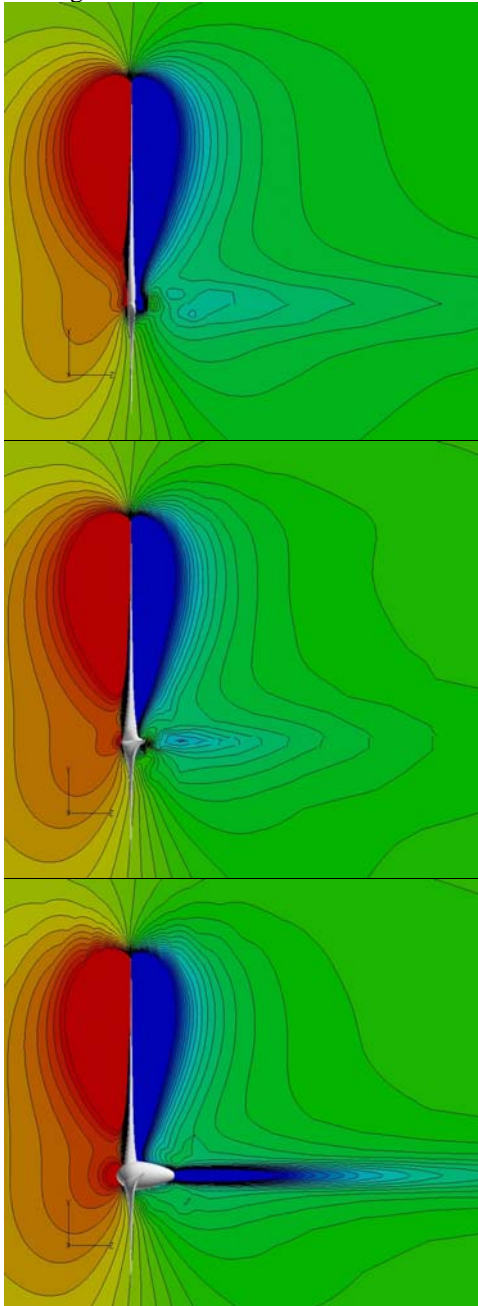


Figure 11: Pressure contours in a vertical plane. Original rotor (top), new design without spinner (middle) and new design with spinner (bottom), $W=8$ m/s, EllipSys3D.

Figure 12 and Figure 13 show contour plots of axial and tangential velocity, respectively. In Figure 12 the red color corresponds to 8 m/s, while blue corresponds to 2 m/s. Here we see the highest velocity deficit at around 70 % radius for all rotors. The presence of the spinner also causes a deficit at the rotational centre.

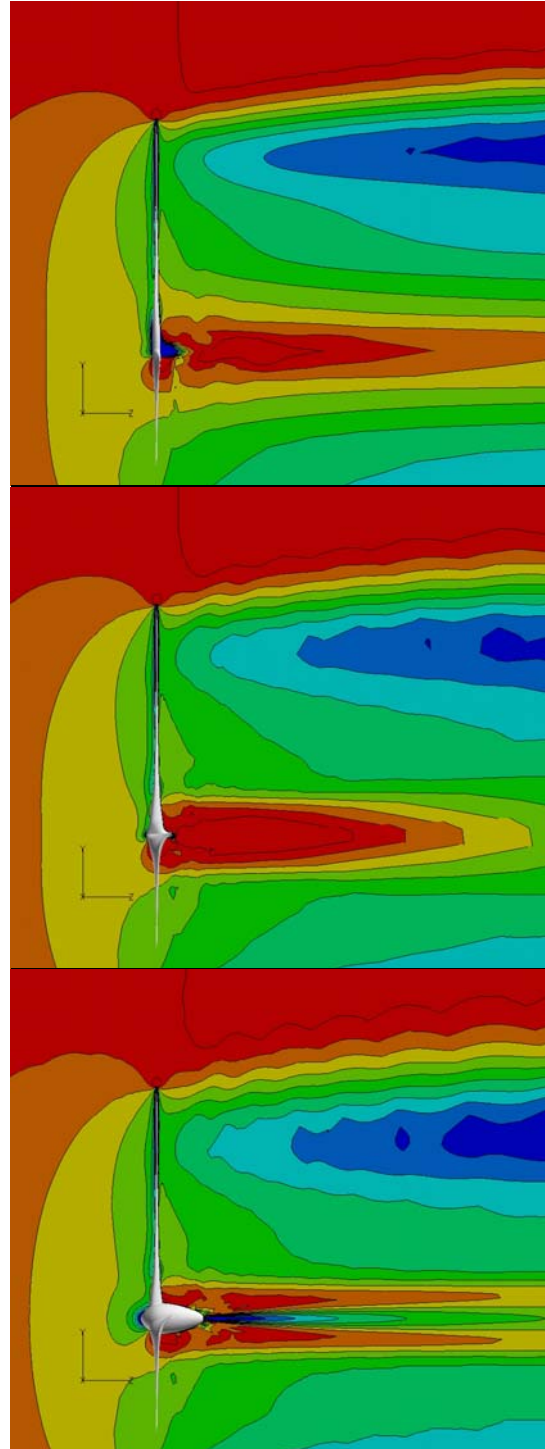


Figure 12: Axial velocity countours in a vertical plane. Original rotor (top), new design without spinner (middle) and new design with spinner (bottom), $W=8$ m/s, EllipSys3D.

In Figure 13 red is positive tangential velocity, while blue is negative velocity. The flow behind the spinner clearly shows an increase in tangential velocity.

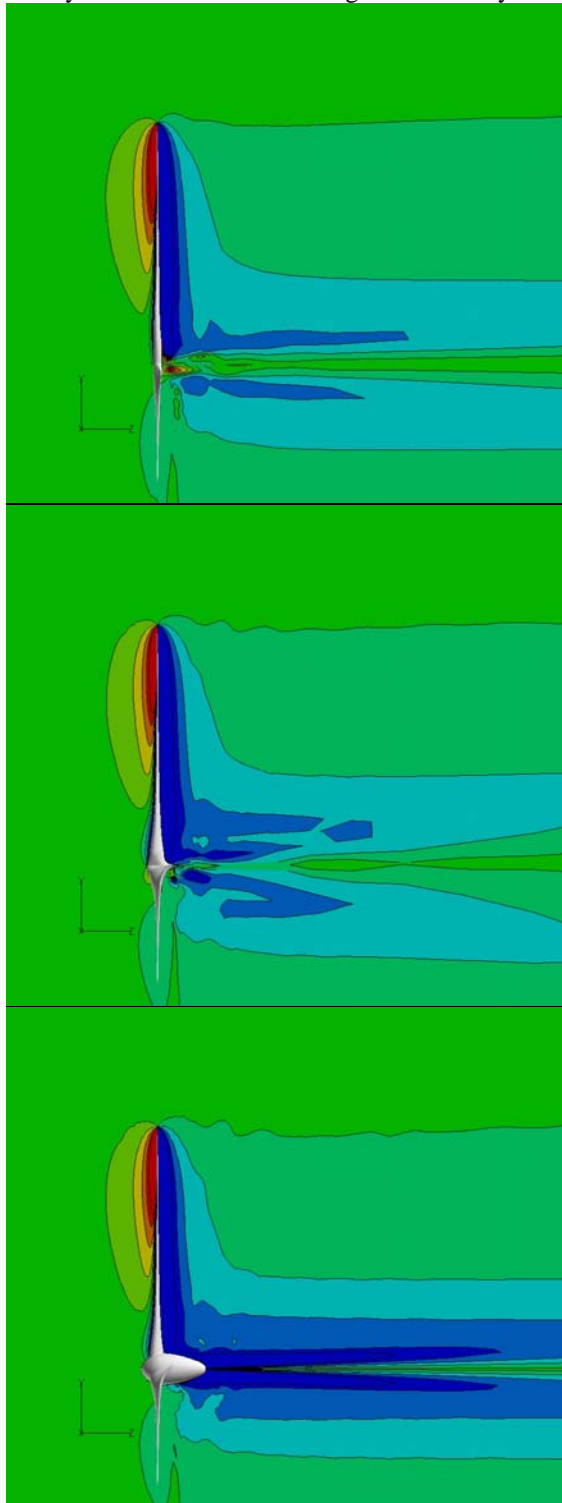


Figure 13: Tangential velocity countours in a vertical plane. Original rotor (top), new design without spinner (middle) and new design with spinner (bottom), $W = 8 \text{ m/s}$, EllipSys3D.

Due to tangential velocity created by the blade and the shape of the spinner the flow will approach the rotation centre with an increasing tangential velocity causing a decrease in pressure.

This will eventually cause an increase in local C_p as seen in the present computations.

Flow visualizations

Figure 14 shows an iso-vorticity surface around the rotor with the large spinner. Here the rotational flow around the rotor centre is seen as a “spiralling” flow around the rotational axis causing the previously mentioned low pressure at the rotation centre.

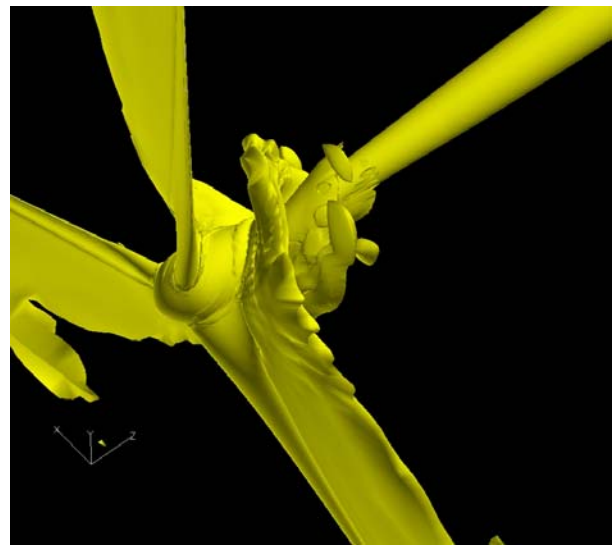


Figure 14: Iso-vorticity surface of flow around the new design with spinner, $W = 8 \text{ m/s}$, EllipSys3D.

Figure 15 shows vorticity contours in a vertical plane through the rotor. The tip vortex is clearly seen as distinct vortices downstream of the tip. Also the spiraling root vortex is seen around the core vortex.

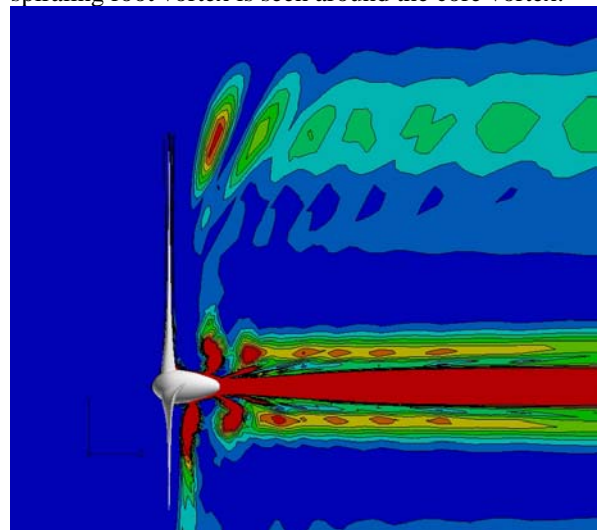


Figure 15: Vorticity contours of flow around the new design with spinner, $W = 8 \text{ m/s}$, EllipSys3D.

Limiting streamlines on the suction side of the rotor geometries are shown in Figure 16.

Here it is seen that the original design (top) results in a separated region on the innermost part of the rotor, while the flow on the two other rotors remain attached.

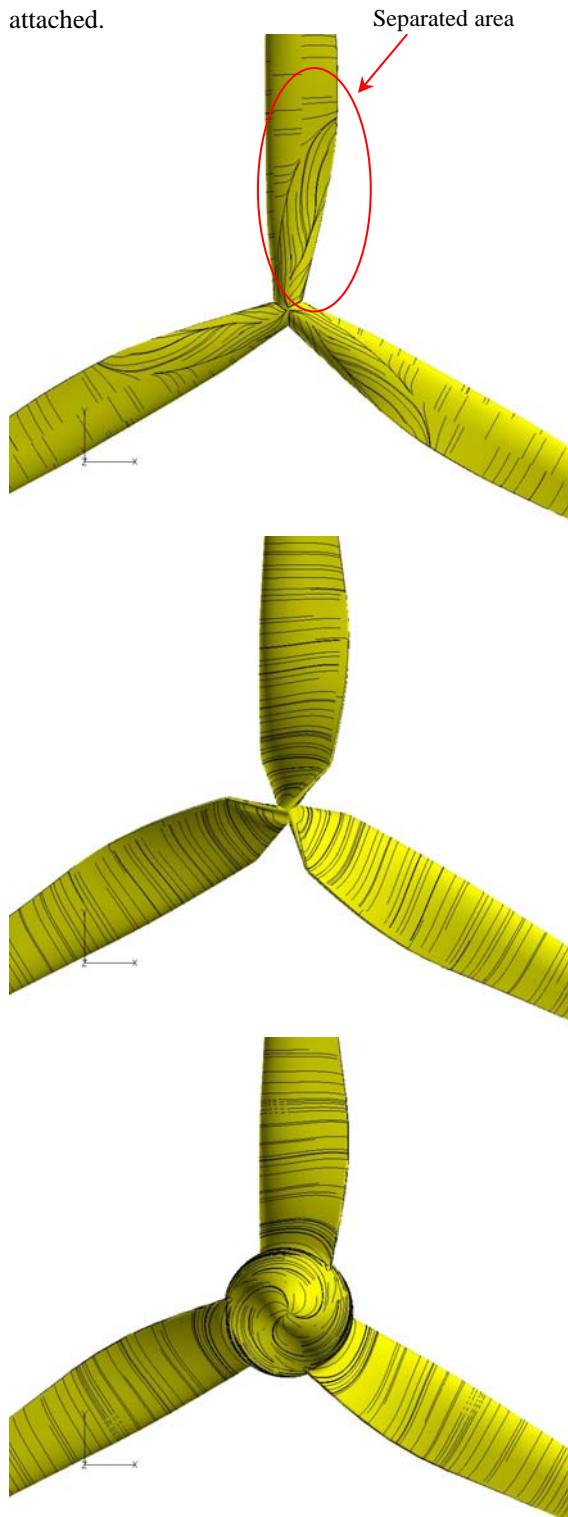


Figure 16: Limiting streamlines on suction side. Original rotor (top), new design without spinner

(middle) and new design with spinner (bottom), $W= 8$ m/s, *EllipSys3D*.

4. Conclusions

Based on a modern Mega-Watt wind turbine rotor design a wind turbine blade has been redesigned and computationally applied on the original rotor. The new blade design has an increased chord and twist distribution towards the centre of rotation. Additionally, the effect of having an “egg-shaped” spinner as a nacelle is investigated.

Three different aerodynamic methods are employed in the present investigation. I.e. the Blade Element Momentum method, The Actuator Disc method and a full 3D Navier-Stokes solver.

Results using the three different aerodynamic methods indicate that:

- A slightly larger mechanical power coefficient, C_p , and thrust coefficient, C_T , are obtained using the new rotor designs as expected due to increase in solidity.
- According to local C_p plots, the Betz limit of $C_p = 16/27$ can be exceeded near the root but will reduce C_p further outboard indicating highly three-dimensional effects
- The pressure contour plots show a low-pressure region at the centre of rotation behind the rotor for the new designs, which is caused by the increase in tangential velocity.
- Finally, visualizations of the limiting streamlines on the surface of the rotors show that the new design do not separate on the suction side at the inner most part, whereas the original blade does.

The present work did show that local C_p differs considerably when comparing BEM with more complex methods as AD and 3D NS. An increase in local C_p on the inboard region cause a decrease further outboard indicating highly three-dimensional effects not accounted for in BEM. This could lead to design changes in future rotor designs. Future work will include aerodynamic optimization for designing a new blade to further investigate these issues.

Acknowledgements

This work was carried out under a contract, ENS-33031-0077, “Research program in applied aeroelasticity”. The CFD computations were made possible by the use of the Risø 240 nodes MARY PC-cluster, and the computational resources of the Danish Centre for Scientific Computing at MEK/DTU in Lyngby.

References

-
- [¹] "Considerably Higher Yields – Revolutionary Rotor Blade Design" WindBlatt 3/2004, Enercon
- [²] de Vries, O. "Fluid Dynamic Aspects of Wind Energy Conversion". AGARDograph No. 243, Report AGARD-AG-243, NATO Research & Technology Association, Neuilly-sur-Seine, France, 1979.
- [³] Petersen, J.T. "The Aeroelastic Code HawC – Model Comparisons". In proceedings of State of the Art of Aeroelastic Codes for Wind Turbine Calculations. 28th Meeting of Experts, International Energy Agency, Annex XI. Editor B. Maribo Pedersen, Technical University of Denmark. Lyngby, April 11-12 1996, pp. 129-135.
- [⁴] Durand W.F. "Aerodynamic Theory". Vol IV, Div. L: Airplane Propellers by H. Glauert, 1935
- [⁵] Madsen, H.A. "Yaw Simulation using a 3D Actuator Disc Model Coupled to the Aeroelastic Code HAWC". Proceedings of the 13th IEA Symposium on the Aerodynamics of Wind Turbines, held at FFA, Stockholm, Sweden November 29-30, 1999.
- [⁶] Aagaard Madsen, H.; Sørensen, N.N.; Schreck, S., "Yaw aerodynamics analyzed with three codes in comparison with experiment." In: AIAA Paper 2003-519. 41. Aerospace sciences meeting and exhibit, Reno (US), 6-9 Jan 2003. (American Institute of Aeronautics and Astronautics, Inc., Reston, VA, 2003)
- [⁷] Michelsen JA "Basis3D - a Platform for Development of Multiblock PDE Solvers.", Technical Report AFM 92-05, Technical University of Denmark, 1992.
- [⁸] Michelsen JA "Block structured Multigrid solution of 2D and 3D elliptic PDE's." Technical Report AFM 94-06, Technical University of Denmark, 1994.
- [⁹] Sørensen NN "General Purpose Flow Solver Applied to Flow over Hills." Risø-R-827-(EN), Risø National Laboratory, Roskilde, Denmark, June 1995.
- [¹⁰] Sørensen, N.N., "Rotor computations using a 'Steady State' moving mesh", IEA Joint Action Committee on aerodynamics, Annex XI and 20. Aero experts meeting, Pamplona (ES), 25-26 May 2005.
- [¹¹] Menter FR "Zonal Two Equation $k-\omega$ Turbulence Models for Aerodynamic Flows". AIAA-93-2906, 1993.
- [¹²] Sørensen NN "HypGrid2D a 2-D mesh generator", Risø-R-1035(EN), Risø National Laboratory, Roskilde, Denmark, 1998